834

Eddy-current computation on a one pole-pitch model of a synchronous claw-pole alternator

Christian Kaehler and Gerhard Henneberger
Department of Electrical Machines (IEM),
Aachen Institute of Technology (RWTH), Aachen, Germany

Abstract *This paper deals with 3D finite-element calculation of eddy currents in the claws of a claw-pole alternator taking the rotational geometry movement into account. Two transient edge-based vector formulations are utilised. The reduction of the model to only one pole pitch in combination with a special boundary pairing in the air gap for the applied lock-step method is presented. Calculations of varying material conductivity are performed with simplified end windings. The speed characteristics of the eddy currents with real conductivity and realistic end windings concludes the paper.*

1. Introduction
Claw-pole alternators are used for the generation of electricity in automobiles. There are three basic requirements to them: the output performance must be improved, the audible noise reduced and the efficiency increased. A description of the magneto-static field calculation, used for output optimisation, and the analysis of the structural-dynamic and acoustic behaviour can be found in the work of Küppers (1996) and Ramesohl (1999).

The efficiency of machines is decreased by different loss mechanisms. In the case of the claw-pole alternator, these are dominantly the ohmic losses in the coils and losses caused by the eddy currents in conducting materials. Both can be broken down into rotor and stator parts. Whereas the ohmic losses can be directly calculated in dependence of the coil currents, an analytic description of the eddy-current losses is not possible.

Finite-element method (FEM) is used to calculate the eddy currents in conducting materials, which are induced by an alternating magnetic field. A time harmonic approach can be applied if the geometry is not shifting, all material properties are linear and sinusoidal currents are used.

In the case of the claw-pole synchronous machine, the rotor is turning with a defined speed while the direct current is used in the excitation coil of the rotor.

In generator mode, the stator coils are driven by three-phase current. All steel materials are non-linear. Therefore, a time-stepping algorithm has to be utilised.

In this paper, the applied transient edge-based $\vec{A}$-approach (Kameari and Koganezawa, 1997) and $\vec{A} - \vec{A}, \vec{T}$-approach (Albertz and Henneberger, 2000) are outlined. The 3D FE model of the claw-pole alternator with one and two pole pitches and also with simplified and realistic end windings are described. Special attention is laid on the meshing strategy required by the pairing algorithm, which defines the rotational movement. The results at load in the generator mode obtained by comparing another model with one pole pitch to a model with two pole pitches are presented. Computations of the one pole-pitch model with varying material conductivity in the claw regions show the application range of both the FE formulations. Calculations on the one pole-pitch model with realistic end windings and real-life material conductivity are performed. The characteristic curve of the eddy-current loss over the alternator speed in the generator mode concludes this paper.

2. Theory of the edge-based solver
The applied edge-based solver is part of an object-oriented solver package (Arians *et al.*, 2001). It applies two different FE eddy-current formulations on simply-connected eddy-current regions.

2.1 $\vec{A} - \vec{A}, \vec{T}$ - formulation
The $\vec{A} - \vec{A}, \vec{T}$-approach presented by Albertz and Henneberger (2000) uses two vector potentials, the magnetic vector potential $\vec{A}$ and the electric vector potential $\vec{T}$, to compute the flux density $\vec{B}$ and the current density $\vec{J}$:

$$\vec{B} = \nabla \times \vec{A}, \quad \vec{J} = \nabla \times \vec{T}. \tag{1}$$

The solver separates the model in the eddy-current free regions Ω_1, where the following equation for $\vec{A}$ is solved:

$$\int_{\Omega_1} \nabla \times \vec{\alpha}_i \cdot \nu \nabla \times \vec{A}(t) \, d\Omega_1 = \int_{\Omega_1} (\vec{\alpha}_i \cdot \vec{J}_0(t) + \nabla \times \vec{\alpha}_i \cdot \nu \vec{B}_r) \, d\Omega_1 \tag{2}$$

and for eddy-current regions Ω_2, the equations read:

$$\int_{\Omega_2} (\nabla \times \vec{\alpha}_i \cdot \nu \nabla \times \vec{A}(t) - \vec{\alpha}_i \cdot \nabla \times \vec{T}(t)) \, d\Omega_2 = 0$$

$$\int_{\Omega_2} \left(\nabla \times \vec{\alpha}_i \cdot \frac{1}{\sigma} \nabla \times \vec{T}(t) + \nabla \times \vec{\alpha}_i \cdot \frac{\partial}{\partial t} \vec{A}(t) \right) d\Omega_2 = 0. \tag{3}$$

$\vec{J}_0(t)$ describes the given coil current density while $\vec{B}_r$ defines remanence. The material parameters ν and σ represent the non-linear reluctivity and

the linear conductivity, respectively. $\vec{\alpha}_i$ defines the shape function of an edge element (in this solver tetrahedra).

The time-stepping algorithm interpolates the time-dependent variables linearly as follows:

$$\vec{A}(t) = \tau \cdot \vec{A}_{n+1} + (1 - \tau)\vec{A}_n \ \text{ ditto for } \ \vec{T}, \vec{J}_0$$

$$\frac{\partial}{\partial t}\vec{A}(t) = \frac{1}{\Delta t}(\vec{A}_{n+1} - \vec{A}_n),$$

(4)

where n represents the number of the transient step, Δt the time in between transient steps and τ the relaxation factor.

To improve the convergence behaviour, the current potential is scaled (Kaehler and Henneberger, 2002). The usual periodic and Dirichlet boundary conditions are used on the model boundaries for $\vec{T}$ and $\vec{A}$. The boundary condition between the eddy-current free regions Ω_1 and the eddy-current regions Ω_2 for the current vector potential reads (Biro and Preis, 2000):

$$\Gamma_{12}: \quad \vec{T} \times \vec{n} = 0,$$

(5)

where $\vec{n}$ is the normal vector of the boundary region. Since in this application all eddy-current regions are continuous and short circuited, equation (5) can easily be achieved by a Dirichlet condition $T_i = 0$ on all edges i of the boundary Γ_{12}.

2.2 $\vec{A}$ - Formulation

The $\vec{A}$-approach applies only the magnetic vector potential $\vec{A}$ in all regions. Here, the formulation for eddy-current regions reads:

$$\int_{\Omega_2} \nabla \times \vec{\alpha}_i \cdot \nu \nabla \times \vec{A}(t) + \sigma \frac{\partial \vec{A}(t)}{\partial t} \, d\Omega_2 = 0,$$

(6)

while the eddy-current free regions are solved with equation (2). The time-stepping algorithm uses equation (4) again. The magnetic flux density $\vec{B}$ and the eddy-current density $\vec{J}$ are computed as follows:

$$\vec{B} = \nabla \times \vec{A}, \quad \vec{J} = -\sigma \frac{A_{n+1} - A_n}{\Delta t}.$$

(7)

In this approach, no boundary conditions have to be applied on the boundaries between the eddy-current and non-conducting regions. Only the usual conditions for $\vec{A}$ on the model boundaries are used.

Since the resulting global FEM matrix for the $\vec{A} - \vec{A}, \vec{T}$-approach is not symmetric, it is solved by the SSOR preconditioner and the TFQMR solver of the ITL package (Lumsdaine *et al.*, n.d). The matrix for the $\vec{A}$-approach is

symmetric, thus allowing the use of the Cholesky-CG combination (Kameari and Koganezawa, 1997) of the same package.

Saturation effects are computed with an overlaying Newton-Raphson procedure for each transient step. The relaxation factor used in between transient steps is chosen as $\tau = 2/3$ (Galerkin-scheme) (Zienkiewicz and Taylor, 1991).

3. Finite element model

Only magnetically relevant components of the synchronous claw-pole alternator are modelled. The end windings is modelled with straight coils or realistically. Since the geometry of the alternator is symmetric over two pole pitches, a 60° model with periodic boundaries can be utilised (Figure 1(b)) (Kaehler and Henneberger, 2002). With antiperiodic boundaries and a special geometric regrouping the model can be reduced to one pole pitch or 30° (Figure 1(a)). Thus, either with the same calculation time denser meshes and therefore smaller Peclet numbers (Rodger *et al.*, 1990) can be computed, or with identical mesh density or Peclet number the number of elements can be halved and the calculation time nearly quartered.

3.1 Winding head

In order to have geometric identity after a rotor movement of one stator-tooth pitch or 10° mechanical, the end windings is simplified as in Figure 1, where each coil runs straight through the whole model. The advantage of this simplification lies in a periodic behaviour of the calculation after 10° and not the usual 60° when taking the end windings into account. Thus, the settling time of calculation can be detected easily.

A model with realistic end windings is shown in Figure 1(c). This model will later be compared to the model with simplified end windings and used when calculating the speed characteristics of the eddy-current loss.

(a)
30° (one pole pitch)

(b)
60° (two pole pitches)

(c)
30° realistic end windings
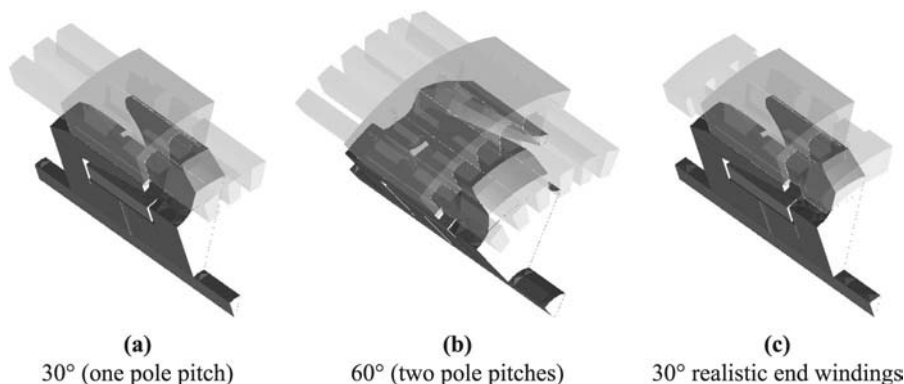
Figure 1.
Models with translucent stator regions and simplified (a,b) and realistic (c) end windings

3.2 Meshing strategy for edge reordering

To represent the rotational movement, a lock-step method is utilised. In this method, no real movement takes place. Instead, boundary conditions are used, which pair edges in each step depending on the rotational angle, while the mesh remains stationary.

This edge-grouping routine of the transient solver depends on a special air-gap discretization. To implement the change of geometry, the FE mesh of the alternator is separated into moving elements in the rotor and stationary elements in the stator. The boundary area of these two meshes is located in the middle of the air gap. It is meshed identically in both separate meshes.

The boundary mesh is partitioned into equidistant areas in the direction of movement. One of these areas (exactly as wide as the step angle) is modelled and meshed in the periodic case (Figure 2(b)). In the antiperiodic case the first area is partitioned into four area meshes, which are created by mirroring (step 1 and 2 in Figure 2(a)). All other meshed areas are generated by symmetric rotation of the first areas (step 3 in both figures). A zoom on the actual antiperiodic boundary mesh in the middle of the air gap of the claw-pole alternator model is shown in Figure 3.

The search function for the pairing of two edges is defined by three vectors. The first $\vec{s}_1$ defines translatory movement in x-, y- or z-direction, the second $\vec{s}_2$ rotational movement around the x-, y- or z-axis and the third $\vec{s}_3$ multiplication of the x-, y- and z-value. With these three vectors translatory as well as rotatory movement can be considered.

In the case of the claw-pole alternator the vectors differ for the two models. In the periodic case (60° or two pole pitches) the search vectors at step n read:

$$\vec{s}_1 = n \cdot \vec{0}, \quad \vec{s}_2 = n \cdot (0°, 0°, 1°)^{\mathrm{T}}, \quad \vec{s}_3 = (1, 1, 1)^{\mathrm{T}}. \tag{8}$$
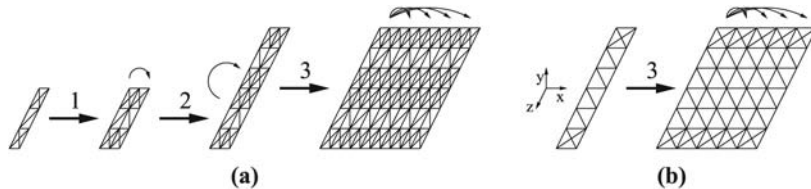
In the antiperiodic case (30° or one pole pitch) the search vectors in periodic regions are identical to (8), while in antiperiodic regions they read:

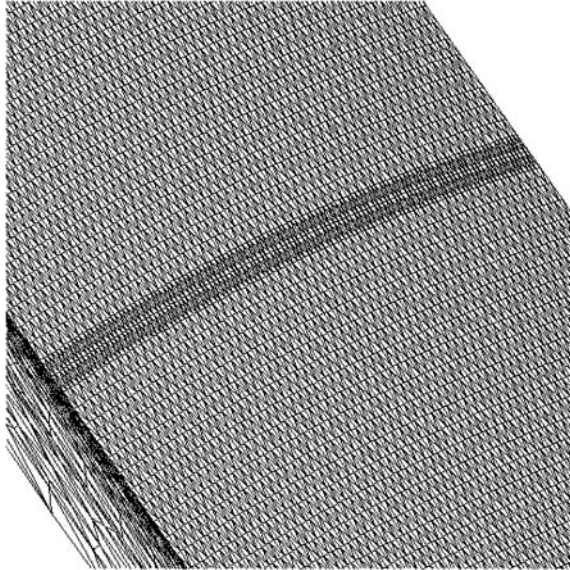$$\vec{s}_1 = n \cdot \vec{0}, \quad \vec{s}_2 = n \cdot (0°, 0°, 1°)^{\mathrm{T}}, \quad \vec{s}_3 = (1, 1, -1)^{\mathrm{T}}. \tag{9}$$

Antiperiodic regions appear when

$$\alpha \cdot (2k - 1) < \vec{s}_2 \cdot (0, 0, 1)^{\mathrm{T}} \leq \alpha \cdot 2k \quad k \in \mathbb{Z}, \tag{10}$$

Figure 2.
Generation of boundary area mesh in air gap. (a) Antiperiodic case, (b) Periodic case

with $\alpha = \alpha_h - \alpha_l = 30°$ being the difference of the lower model boundary $\alpha_l = 75°$ and the higher boundary $\alpha_h = 105°$.

The corresponding edges are detected by the position of their nodes. They can be inserted into the FEM matrix as periodic or antiperiodic boundary conditions.

Since the edge directions change in the antiperiodic case, due to the negative sign of $\vec{s}_3$ in equation (9), the directions of the fluxes also change automatically in these regions for the claw-pole alternator. Thus, all paired edges are inserted as periodic binary constraints into the FEM matrix.

4. Calculations and results

The calculations are conducted at constant speed. The mechanical step angle amounts to $\alpha = 1°$, leading to, for example, $\Delta t = 55.556\,\mu s$ in between transient steps for a speed of $n = 3,000\,rpm$. The excitation current is impressed in the rotor. The three-phase current of the real alternator in generator mode is injected in the stator coils. It turns synchronously with the rotor.

The calculations on the 30° and the 60° model are compared at low material conductivity, proving that the use of the smaller antiperiodic model yields correct results. The conductivity is varied up to the real material conductivity of the claws utilising both transient formulations. The computations with simplified and realistic winding differ only in the average eddy-current loss

value. Finally, the speed characteristic of the average eddy-current loss with realistic end windings in generator mode is determined.

*4.1 Comparison of one and two pole-pitch model*
For the comparison of the one and the two pole-pitch model (Figure 1(a) and (b)) a low material conductivity of $\sigma = 4.0 \times 10^2$ $(\Omega\,\mathrm{m})^{-1}$ and the $\vec{A} - \vec{A}$, $\bar{T}$-approach are selected, since in this calculation the exact value of the eddy currents is not of interest, but the difference in between the model solutions.

The total eddy-current loss in the claws over the rotation is shown in Figure 4 for both models. Additionally, the relative difference is shown on the secondary axis. After a short settling time of about 15 time steps, a periodicity of the eddy-current losses of $\Delta\alpha = 10°$ mechanical occurs, as expected for the simplified end windings. The eddy-current distributions for both the models for a specific time step are shown in Figure 5 on the same scale. The maximum eddy-current values as well as the maximum magnetic flux densities are located on the lower flank of the claw (generator effect), the rotor turning mathematically positive.

The calculation of the average energy density $\bar{w}$ of the eddy currents over a period of the losses leads to Figure 6:

$$\bar{w} = \frac{\Delta t}{\sigma} \sum_{n=1}^{N} \vec{J}_n^2, \qquad (11)$$

with N being the number of steps in a period and $\vec{J}_n$ the eddy-current density of that element at step n. Again the maximum is located on the lower flank.
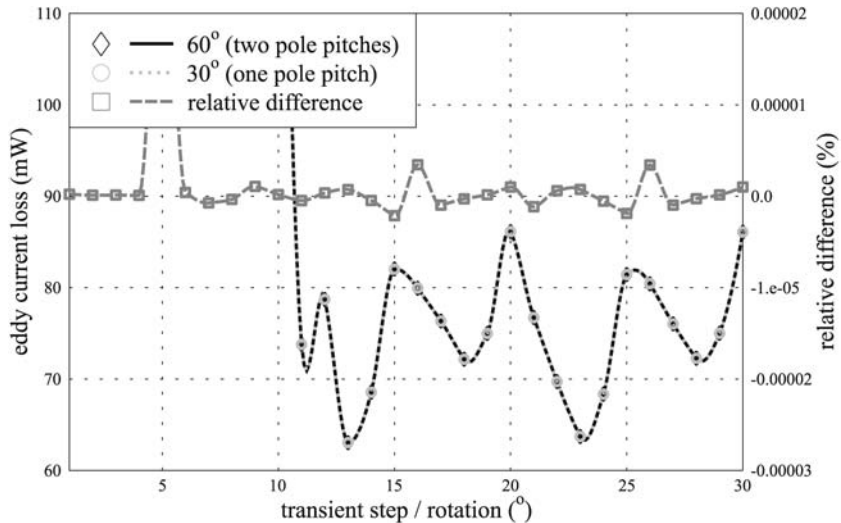
Figure 4.
Eddy-current loss vs rotation for material conductivity $\sigma = 4.0 \times 10^2$ $(\Omega\,\mathrm{m})^{-1}$ at constant speed $n = 3,000\,\mathrm{rpm}$

(a) 30° (one pole pitch)

(b) 60° (two pole pitches)
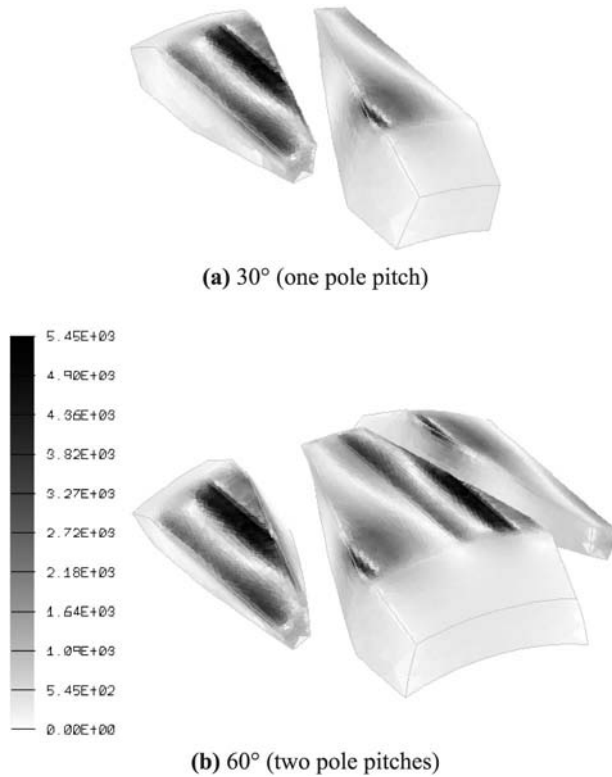
Figure 5.
Eddy-current
distribution J (A/m^2) at
step 25 for conductivity
$\sigma = 4.0 \times 10^2$ (Ω m)$^{-1}$
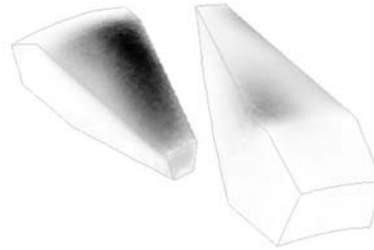and speed $n = 3{,}000$ rpm

The local differences between both the models are caused by the differences in the mesh density.

The distribution of the average loss in energy can later be used as excitation for thermal solvers. Since the thermal distribution will only differ by diffusion effects from the energy distribution, the maxima distributions in Figure 6(a) and (b) can already be compared to hotspot distributions in temperature measurements on the surfaces of the rotor claws.

The global results (relative difference $\varepsilon < 10^{-5}$ per cent) as well as the eddy-current density and energy distributions are close to identical, proving the eddy-current distribution as well as the magnetic flux density to be antiperiodic in the one pole-pitch model. With this model, the element number can be reduced by a factor of two, although the mesh density and the local error stays identical in all model regions. Thus, the number of unknowns is nearly halved and the calculation time about quartered.

Since it has been proven that calculations on one pole-pitch models yield correct results, all further calculations are conducted on these models due to their shorter calculation time.

(a) 30° (one pole pitch)
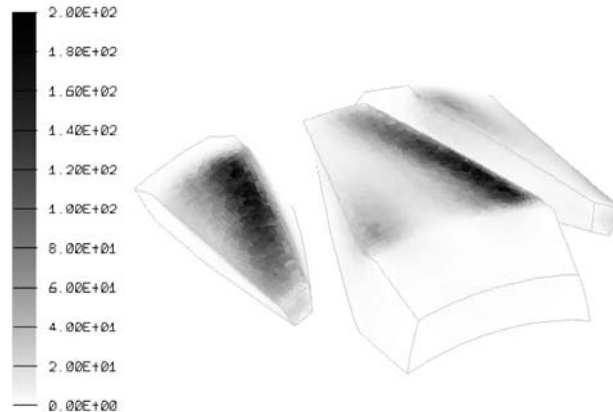
(b) 60° (two pole pitches)

Figure 6.
Average eddy-current
energy distribution
$\bar{w}$ (W/m^3) for
conductivity
$\sigma = 4.0 \times 10^2$ $(\Omega\,\text{m})^{-1}$
and speed $n = 3,000\,\text{rpm}$

4.2 Variation of material conductivity in the claws
The material conductivity in the claws is varied using both transient formulations, beginning with the $\vec{A} - \vec{A}$, $\vec{T}$-approach for low and using the $\vec{A}$-formulation for high material conductivity.

In order to achieve smooth convergence and to reduce the settling time, the computation with the $\vec{A} - \vec{A}$, $\vec{T}$-approach is started with the material conductivity of the claws being $\sigma = 4.0 \times 10^2$ $(\Omega\,\text{m})^{-1}$ or Peclet number Pe $\approx$ 0.001, which is defined as (Rodger *et al.*, 1990):

$$\text{Pe} = \frac{vl\mu\sigma}{2}. \tag{12}$$

In equation (12) v represents the velocity, l the characteristic length of an element in the direction of movement and μ the permeability of the element material.

The conductivity is subsequently increased to $\sigma = 1.0 \times 10^6$ $(\Omega\,\text{m})^{-1}$ or Pe $\approx$ 2.5 as depicted in Figure 7. The real conductivity of $\sigma = 4.0 \times 10^6$ $(\Omega\,\text{m})^{-1}$ (Pe $\approx$ 10) leads to divergence when using the $\vec{A} - \vec{A}$, $\vec{T}$-formulation.
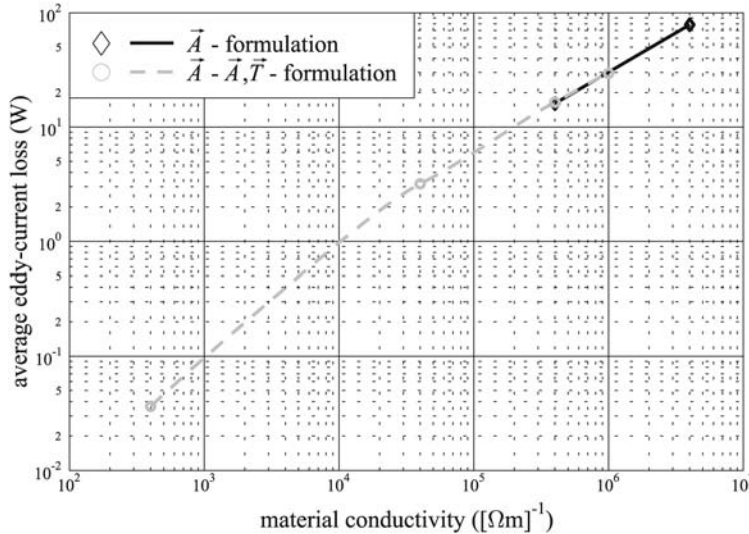
Therefore, the simulation is finished with the $\vec{A}$-approach which only converges for high material conductivities. Here, the material conductivities $\sigma = 4.0 \times 10^5$ $(\Omega\,\mathrm{m})^{-1}$ (Pe ≈ 1) and $\sigma = 4.0 \times 10^6$ $(\Omega\,\mathrm{m})^{-1}$ (Pe ≈ 10) are computed.

In the $\vec{A}$-approach, it is essential to start with a static step since otherwise the eddy currents rise dramatically in the first step. Without static start step the solver computes the eddy currents that would build-up, if the machine started from no excitation and zero speed to full excitation and full speed in one time step. The relaxation time would then prolong to about 100 transient steps. With static start step, the computation simulates the spontaneous change from zero to full conductivity of the claw-pole material. Here, the relaxation time of about 15 transient steps is comparable to the relaxation time of the $\vec{A} - \vec{A}$, T-approach.

The average total eddy-current loss over the material conductivity of the whole generator is depicted on a logarithmic scale in Figure 7. Both transient formulations show a nearly potential dependency of the eddy currents on the material conductivity of the claw.

4.3 Comparison of simplified and realistic winding head

The two models of one pole pitch with simplified and realistic end windings (Figure 1(a) and (c)) yield slight differences in the total eddy-current loss when computed with the $\vec{A}$-formulation.

Both models are identically meshed in all regions. The different coil topology is generated by different material definitions in the winding-head regions of the stator mesh. Thus, the differences are only caused by the winding-head definition and not by the discretization.

The periodicity of the simplified end windings is congruent with the assumptions taken in Section 3. As shown in Figure 8, the loss period amounts to the expected 10° mechanical or 10 transient steps. Due to the three-phase current in the end windings of the wave winding in the stator, the periodicity of the model with realistic end windings also amounts to 10° mechanical or 10 transient steps. In this model, the current distribution in the end windings is also periodic over 10° mechanical. Therefore, the magnetic flux and the eddy-current distributions follow the same period.

The slight differences are caused by the differing coil-current path in the stator regions. The average eddy-current loss of the model with realistic end windings is about 2 per cent lower than the loss of the model with simplified windings.

4.4 Speed characteristic of the eddy-current loss
The main aim of the transient calculations lies in determining the eddy currents of the real claw-pole machine for all working points.

In order to do so, the material conductivity of iron $\sigma = 5.0 \times 10^6\ (\Omega\,\mathrm{m})^{-1}$ at temperature $T = 175°C$ is used for the massive steel regions of the claws. Thus, the Peclet number amounts to $\mathrm{Pe} \approx 12.5$.

The $\vec{A}$ - approach is applied on the 30° model with realistic end windings (Figure 1(c)). The stator currents in generator mode at constant excitation in the rotor of $I_f = 4\,\mathrm{A}$ are impressed into the stator coils. The constant alternator speed is varied from $n = 1,500$ to $6,000\,\mathrm{rpm}$ as shown in Figure 9. The resulting average eddy-current energy for $n = 6,000\,\mathrm{rpm}$ is shown in Figure 10.

The result leads to the characteristic speed curve of the average eddy-current loss of the synchronous claw-pole alternator in generator mode
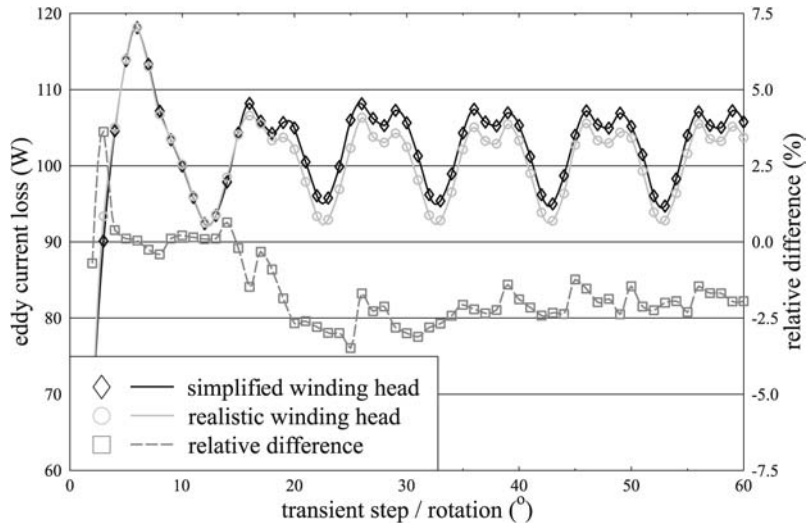
Figure 8.
Eddy-current loss vs rotation with simplified and realistic end windings for material conductivity $\sigma = 4.0 \times 10^6\ (\Omega\,\mathrm{m})^{-1}$ at constant speed $n = 3,000\,\mathrm{rpm}$
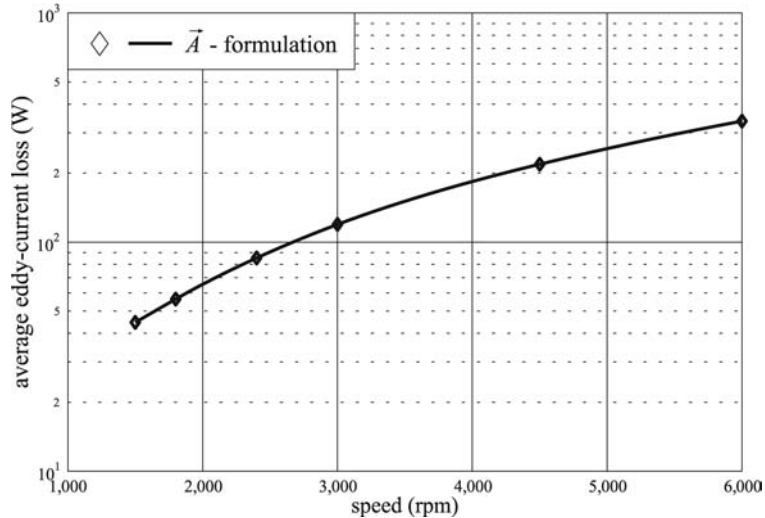
Figure 9.
Eddy-current loss vs
alternator speed for
material conductivity
$\sigma = 5.0 \times 10^6 \, (\Omega \, \text{m})^{-1}$ in
generator mode
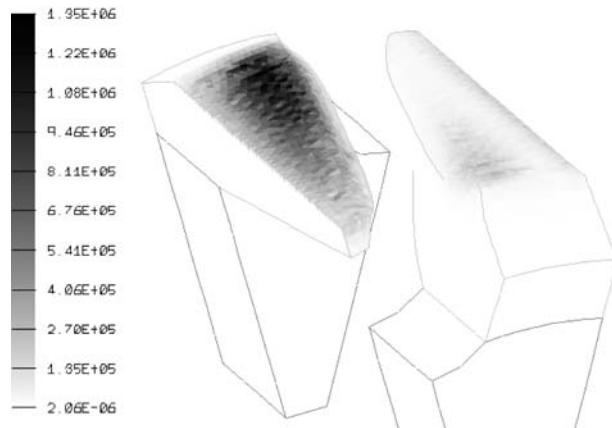
Figure 10.
Average eddy-current
energy $\bar{w}$ (W/m^3) at
speed $n = 6{,}000$ rpm for
material conductivity
$\sigma = 5.0 \times 10^6 \, (\Omega \, \text{m})^{-1}$

on a half-logarithmic scale is shown in Figure 9. This speed characteristic of the loss can later be used in electric circuit or domain simulations of the alternator and of the whole automobile.

5. Conclusions

In this paper, a transient 3D FEM to calculate the eddy currents in the claws of a synchronous claw-pole alternator is presented taking the rotational movement and two edge-based vector formulations into account.

Special attention has been laid on the comparison of a one and a two pole-pitch model and their meshing strategy in the air gap. Both models yield identical eddy-current and average energy distributions, which have been

depicted in this paper. Thus, by the use of antiperiodic edge grouping, the number of unknowns has been reduced by about a factor of two without loosing precision.

On the smaller model with one pole pitch, calculations with varying material conductivity have been performed showing the potential dependency of the eddy-current loss on the conductivity of the claws and the application range of the two transient formulations.

Additionally, two models of one pole pitch with simplified and realistic end windings have been compared. While their periodicity stays identical, the average eddy-current loss with realistic end windings is slightly lower.

Last, the speed characteristic in generator mode of the average eddy-current loss as well as the average eddy-current energy at speed $n = 6,000$ rpm on the rotor claws with realistic material conductivity and end windings has been calculated and presented.

References

Arians, G., van Riesen, D. and Henneberger, G. (2001), "Innovative object oriented environment for designing different finite element solvers with various element types and shapes," *Record of the 13th Compumag Conference on the Computation of Electromagnetic Fields*, Evian, France, July 2001, Compumag, Vol. II, pp. II218-19.

Albertz, D. and Henneberger, G. (2000), "On the use of the new edge based $\vec{A}, -\vec{A}, \vec{T}$, formulation for the calculation of time-harmonic, stationary and transient current field problems", *IEEE Transactions on Magnetics*, Vol. 36 No. 4, pp. 818-22.

Biro, O. and Preis, K. (2000), "An edge finite element eddy current formulation using a reduced magnetic and a current vector potential", *IEEE Transactions on Magnetics*, Vol. 36 No. 5, pp. 3128-30.

Kaehler, C. and Henneberger, G. (2002), "Eddy current computation in the claws of a synchronous claw pole alternator in generator mode", *IEEE Transaction on Magnetics*, Vol. 38 No. 3, pp. 1201-4.

Kameari, A. and Koganezawa, K. (1997), "Convergence of ICCG method in FEM using edge elements without gauge condition", *IEEE Transactions on Magnetics*, Vol. 33 No. 2, pp. 1223-6.

Küppers, S. (1996), "Numerische Verfahren zur Berechnung und Auslegung von Drehstrom-Klauenpolgeneratoren (Numerical methods for the calculation and design of three-phase claw-pole alternators)", PhD thesis, Department of Electrical Machines, Aachen Institute of Technology, Shaker verlag, Aachen.

Lumsdaine, A., Siek, J. and Lie-Quan Lee, "The iterative template library - itl", Available: http://www.lsc.nd.edu/research/itl, [Online]

Ramesohl, I. (1999), "Numerische Geräuschberechnung von Drehstrom-Klauenpolgeneratoren (Numerical acoustic cal-culation of tree-phase claw-pole alternators)", PhD thesis, Department of Electrical Machines, Aachen Institute of Technology, Shaker verlag, Aachen.

Rodger, D., Leonhard, P.J. and Karaguler, T. (1990), "An optimal formulation for 3D moving conductor eddy current problems with smooth rotor", *IEEE Transactions on Magnetics*, Vol. 26, pp. 2359-63.

Zienkiewicz, O.C. and Taylor, R.L. (1991), *The Finite Element Method*, McGraw-Hill Book Company, London, New York.